Available online at www.sciencedirect.com
ScienceDirect
Journal of the European Ceramic Society 28 (2008) 2915–2921
www.elsevier.com/locate/jeurceramsoc

Preparation and characterization of zinc hydroxide carbonate and porous zinc oxide particles

M. Bitenc [a], M. Marinšek [b], Z. Crnjak Orel [a,*]

[a] *National Institute of Chemistry, Hajdrihova 19, SI-1000 Ljubljana, Slovenia*
[b] *Faculty of Chemistry and Chemical Technology, Aškerčeva 5, SI-1000 Ljubljana, Slovenia*

Received 10 March 2008; received in revised form 5 May 2008; accepted 9 May 2008
Available online 1 July 2008

Abstract

A simple urea aqueous solution process at low temperature (85 °C) was employed for the preparation of zinc hydroxide carbonate from zinc nitrate. The influence of different additives on the final particle morphology was studied. Porous spherical particles in the shape of chrysanthemums with an average size of 4 μm and a surface area of 16 m^2/g were obtained in the presence of poly-vinyl pyrrolidone (PVP-K30). After heat treatment ZnO particles were formed that preserved the size and shape of the hydrozincite precursor. The morphology and crystallinity of the solids obtained before and after the heat treatment were characterized by FE-SEM, XRD, FTIR, BET and TG methods.

Keywords: ZnO; Powder-chemical preparation; Electron microscopy; Thermal properties; Particle size

1. Introduction

Zinc oxide (ZnO), due to its specific chemical, surface and microstructural characteristics, can be used in a wide range of applications, including the manufacture of varistors, protective elements in electric and electronic appliances, as gas-sensors, catalysts, in the pigment industry as a colour hue, in cosmetics as a UV light absorber, etc.[1,2] In literature many preparative techniques for ZnO are described. For preparation of ZnO nanostructure rods, a vapour-phase transport process in the presence of noble metal catalysts and thermal evaporation are the two major vapour techniques.[3–6] Larger scale ZnO preparation can be achieved by chemical solution routes.[7–10] A frequently used method is precipitation from an aqueous solution of a Zn–salt in the presence of ammonium carbonate or urea, yielding a hydroxide carbonate precursor. The latter is then transformed into ZnO by thermal decomposition.

The composition and properties of the precipitated zinc hydroxide carbonate are largely dependent on the precipitation conditions, which also influence the final ZnO morphology.[11] However, systematic studies of the morphological modulation of Zn-based precipitates with different additives in aqueous solution in the literature are still incomplete. In this respect, it is necessary to find the relationship between added surface agents and the morphologies of the precipitated Zn-based precursors in order to develop an effective and simple route for controlling the final ZnO characteristics such as shape and size. Regarding final powder shape, ZnO microparticles with new morphologies (nut-like or rice-like) have been obtained from aqueous solution with the assistance of different additives. Recently the formation mechanism of ZnO nanoparticles prepared by the homogeneous precipitation method using urea and zinc nitrate was discussed by Liu et al.[12] In the article it was shown that first $Zn_4CO_3(OH)_6{\cdot}ZnO$ is formed and after heating at 500 °C it decomposed in to ZnO.

The mechanism and kinetics of the thermal decomposition of precipitated zinc precursors were reported by several authors. One of the earlier studies on the thermal decomposition of hydrated zinc carbonate ($ZnCO_3{\cdot}2ZnO{\cdot}2H_2O$) was performed by Dollimore et al.[13] On the basis of isothermal TG in the temperature range 200–260 °C they reported an activation energy of 94 ± 9 kJ/mol for two thermally overlapping stages during the decomposition. On the basis of DTA results Chen et al.[14] reported a single step decomposition process with an activation energy of 113 kJ/mol for thermal decomposition of $Zn_4CO_3(OH)_6{\cdot}H_2O$.[14] A single-step decomposition of pure

* Corresponding author. Tel.: +386 1 476 0 236; fax: +386 1 476 0 300.
E-mail address: zorica.crnjak.orel@ki.si (Z. Crnjak Orel).

0955-2219/$ – see front matter © 2008 Elsevier Ltd. All rights reserved.
doi:10.1016/j.jeurceramsoc.2008.05.003

and industrially prepared zinc hydroxide carbonate to ZnO with little change in its overall morphology and an apparent activation energy of 123 and 153 kJ/mol, respectively, was also suggested by Kanari et al.[15] In agreement with some other earlier studies, they also suggested a "nucleation and growth" mechanism for ZnO preparation during the thermal decomposition of the precipitated zinc precursors. A similar value (129 kJ/mol) regarding the apparent activation energy for $Zn_4CO_3(OH)_6$ thermal decomposition was also reported by Li et al.[16] who used a non-isothermal kinetic approach. They suggested that zinc hydroxide carbonate thermal decomposition is a double-step reaction of two-dimensional diffusion followed by irreversible decomposition.

In this paper, we describe a simple urea aqueous solution route for the synthesis of zinc hydroxide carbonate and ZnO microcrystals using zinc nitrate as the starting salt. The morphological characteristics of the Zn-based precipitates were altered by small additions of different additives like PVP, SDS, AA, Triton-X100 and β-CD. By always using the same preparation technique we tried to elucidate the role of different surface active agents during solid phase formation. Different spectroscopic techniques were used for product characterization such as FE-SEM, XRD, BET and IR. In addition, the paper also focuses on the thermal decomposition behaviour of differently prepared and well-characterized zinc hydroxide carbonate ($Zn_5(OH)_6(CO_3)_2$).

2. Experimental method

All reagents in the experimental work were of analytical reagent grade. To avoid hydrolysis upon storage, fresh stock solutions prepared from $Zn(NO_3)_2{\cdot}6H_2O$ (Aldrich) and urea (Aldrich) in millique water were used. In all experiments the initial concentrations of Zn^{2+} ions and urea were 0.01 and 0.05 M, respectively. Experiments were performed without and in the presence of different surface active agents such as PVP-K30, SDS, Triton X-100, β-CD and L-AA. All additives were dissolved in the initial reactive mixture before hydrolysis took place. Two different concentrations of additives were used (0.5 or 3 mg/mL) throughout the experimental study. The experiments were carried out in 14 mL closed reactors, where the total volume of reaction mixture was 10 mL. All experiments were performed in an oven, preheated at 90 °C. During these experiments, the temperature was measured in the centre of test tube with a Fluke 54 II thermocouple type K with thickness of 1 mm. The resulting temperature profile[17] shows that maximum temperature is reached after around 100 min and was constant (85 °C) during the synthesis. The resulting solids were filtered off, washed with water and dried in air. The most promising samples were subsequently thermally treated in Ar at 600 °C for 30 min.

All samples were characterized by scanning field emission electron microscopy (FE-SEM, Zeiss Supra 35 VP with an EDS analyzer). X-ray diffraction analyses (XRD) were carried out on a Siemens D-500 X-ray diffractometer. XRD data were used to obtain the mean crystallite size and microstrain (PANalytical program X'Pert HighScore with Scherrer algorithm) where instrumental broadening corrections were performed using a standard of Al_2O_3. IR spectra were obtained on an FTIR spectrometer (PerkinElmer 2000) in the spectral range between 4000 and 400 cm^{-1} with a spectral resolution of 2 cm^{-1} in the transmittance mode. The KBr pellet technique with about 1 wt% of sample was used for sample preparation. BET measurements were performed using a Micromeritics Gemini II 2370 Surface Area Analyzer. The samples were dried and degassed at 90 °C in a Micromeritics Flow prep 060 module. The Gemini II 2370 performs fully automatic analysis in ultra-high purity nitrogen (99.9995), collects data and performs calculations to obtain the BET surface area.

Thermogravimetric decomposition experiments were performed using 5 mg of sample and a NETZSCH STA 449 °C set-up with a microbalance having a sensitivity of ±0.1 μg. All the experiments were carried out at a constant flow of Ar (50 mL/min). For kinetic analysis TG experiments were repeated under non-isothermal (heating rate 5 °C/min in the temperature range 30–400 °C) and isothermal conditions. Isothermal tests always started with a non-isothermal period. The starting temperature of the isothermal period was chosen on the basis of the results of the non-isothermal tests where the decomposition reaction at the beginning of the isothermal period in neither case exceeded ∼25% (∼6.5% of the total mass).

3. Results and discussion

The FE-SEM micrographs of six samples prepared after 4 h of synthesis at 85 °C with and without various additives are presented in Fig. 1. The concentration of additives was kept at 3 mg/mL. On addition of ascorbic acid at this concentration no products were obtained, and for that reason a lower quantity of ascorbic acid (0.5 mg/mL) was used in further experiments as presented in Fig. 1f. The products obtained were reproducible when the synthesis was performed under the same conditions.

The micrographs in Fig. 1a–d show porous spherical particles in the shape of a chrysanthemum, while Fig. 1e shows product in the shape of agglomerated leaves. Non-porous spherical particles less than one micrometer in size were obtained after addition of ascorbic acid (Fig. 1f). Products obtained without any additives, as well as with added β-CD or Triton-X100, were porous and not homogeneous. When PVP-K30 was added the products obtained were very homogeneous, in the shape of a spherical chrysanthemum with an average diameter around 4 μm.

When a lower concentration of PVP-K30 (0.5 mg/mL) was added (Fig. 2a), the obtained product was no longer homogeneous and its average particle size increased to 6 μm. The shape and size of the particles were much more similar to those obtained in reaction without additives (Fig. 1a). Similarly, changes in the particle morphology were also noticed with a lower concentration of SDS in the initial reaction mixture. At 0.5 mg/mL of added SDS the leaves obtained were thinner and agglomerated into spherical groups (Fig. 2b). On the contrary, at lower concentrations of added β-CD or Triton-X100, no significant changes were observed regarding the shape and size of the precipitated products. The above facts imply that PVP, SDS and

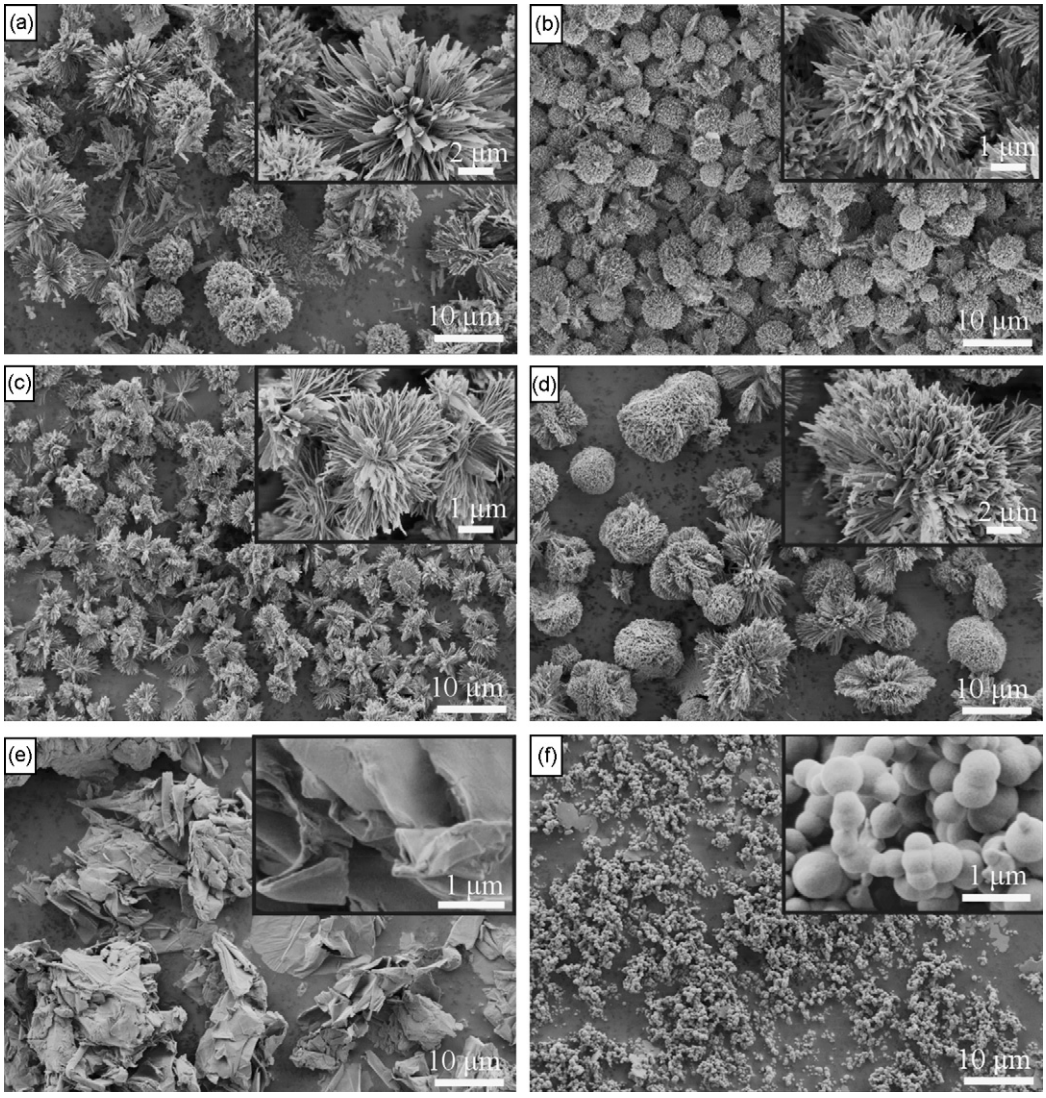

Fig. 1. FE-SEM micrographs of samples prepared after 4 h of synthesis at 85 °C with different additives: (a) no additive; (b) PVP-K30 3 mg/mL; (c) β-CD 3 mg/mL; (d) Triton X-100 3 mg/mL; (e) SDS 3 mg/mL; (f) AA 0.5 mg/mL.

AA have the greatest influence on product morphology. However, the origin of system stabilization may be very different in all three cases. AA is a well known complexing agent and may inhibit new solid phase precipitation through relatively stable complex formation in the precursor solution. PVP and SDS, on the other hand, adsorb to charged solid surfaces owing to their polarity. This leads to coating formation which influences subsequent particle growth.

Since the most homogeneous products were obtained after the addition of 3 mg/mL PVP-K30 to the reaction system,

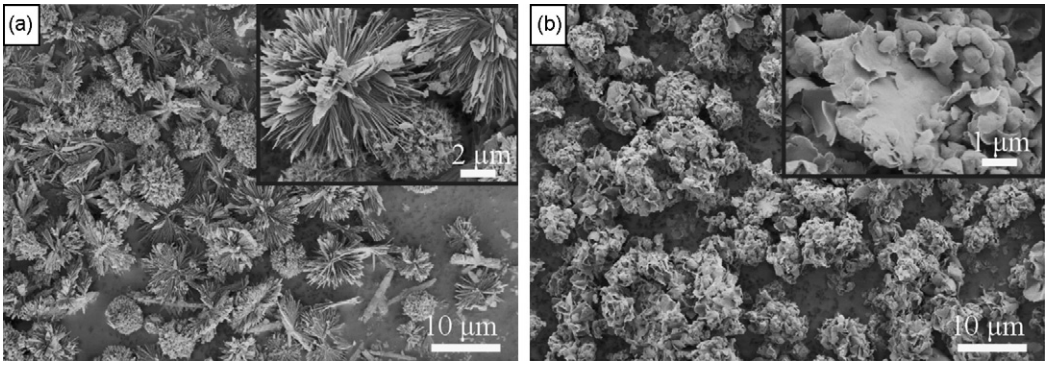

Fig. 2. FE-SEM micrographs of samples prepared after 4 h of synthesis at 85 °C with different additives: (a) PVP-K30 0.5 mg/mL; (b) SDS 0.5 mg/mL.

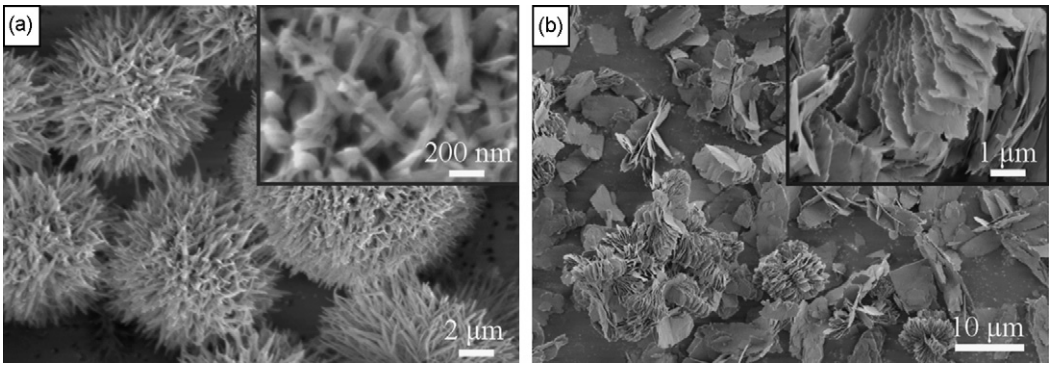

Fig. 3. FE-SEM micrographs of samples prepared at 85 °C with 3 mg/mL added PVP-K30 after: (a) 3 h; (b) 24 h of synthesis.

we focused on the optimization of the parameters for their preparation. When the particle morphology was followed with time, the formation of porous spherical particles was monitored after 3, 4 and 24 h of reaction. Figs. 1b and 3a and b show that the general shape of the precipitated solid phase changed. It is known that urea decomposes very slowly at temperatures under 70 °C. The optimum temperature for urea hydrolysis is at about 85 °C, which was reached in our system after around 100 min.[17] For that reason the formation of solid phase is relatively slow at the beginning of the experiment and substantially faster after a certain induction time needed for rapid urea decomposition. From the SEM investigations it was found that the kinetics of solid phase formation influences the precipitated particle morphology. The porous spherical particles obtained after 3 h of reaction were composed of nanowires (Fig. 3a). After 4 h (Fig. 1b) the wires grew in one dimension—becoming wider but the shape of the particles remained spherical. After 24 h (Fig. 3b) of reaction, the needle-like elements become wider (leaf-like). Some of the particles were still spherical, but most of them were agglomerates composed of leaves.

Samples without any additives (reference sample) and with 3 mg/mL of added PVP-K30 (most homogeneous sample) were also characterized by FTIR, XRD, TG and BET.

The FTIR spectrum of a sample prepared after 4 h of synthesis with added PVP-K30 is presented in Fig. 4a. The presence of carbonate groups in the product was confirmed by bands in the range from 1600 and 1200 cm^{-1} (ν_3 frequency) and 1044, 831 and 708 cm^{-1} (ν_1 frequency). According to the literature[11,18] these bands can also be used for microstructural characterization of precipitated $Zn_5(OH)_6(CO_3)_2$. Musić et al.[11] used the splitting of the ν_3 frequency of the bands at 1512 and 1387 cm^{-1} to confirm microstructural changes in precipitated $Zn_5(OH)_6(CO_3)_2$ obtained under different conditions. More crystalline $Zn_5(OH)_6(CO_3)_2$ was reflected in additional separation and sharpening of the spectral lines. Since our sample (3 mg/mL of added PVP-K30; Fig. 4a) showed only bands at 1560, 1511, 1420 and 1383 cm^{-1}, we deduced that the sample was not well crystallized but rather mostly in an amorphous state. After thermal treatment (600 °C) of the precipitate the band at 425 cm^{-1} with a pronounced shoulder at 560 cm^{-1} in the IR spectra (Fig. 4b) confirmed the presence of ZnO. Again, IR spectra showing characteristic bands of ZnO in the region from 680 up to 300 cm^{-1} can be used not only for qualitative characterization but also for confirmation of the shape of ZnO particles.[18,19] In the work of Verges et al.[20] it was shown that for spherical particles an IR band at 458 cm^{-1} was obtained and that it splits into two bands when the shape was changed. For a prismatic microstructure they obtained two well split bands at 512 and 406 cm^{-1}. In our work the obtained bands at 425 and 560 cm^{-1} confirmed the presence of leaf-like particles agglomerated into spheres.

XRD spectra of a sample prepared with PVP-K30 additive before and after heat treatment are presented in Fig. 5. From

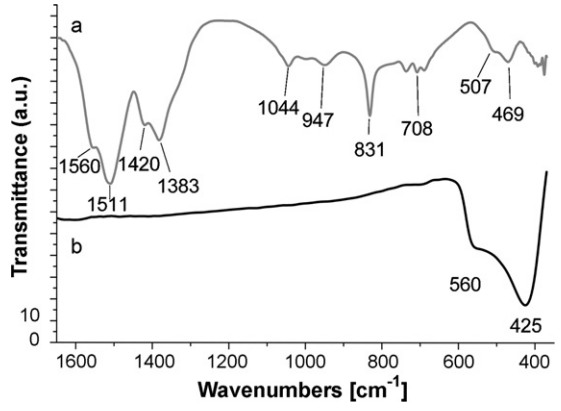

Fig. 4. FTIR spectra of samples prepared after 4 h of synthesis with added PVP-K30 (3 mg/mL): (a) as prepared; (b) after heat treatment.

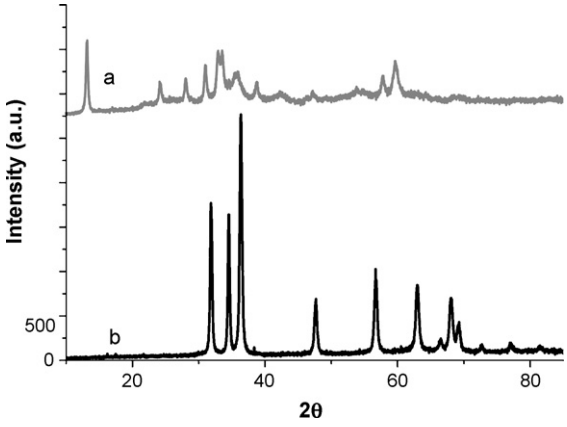

Fig. 5. XRD spectra of a sample prepared after 4 h of synthesis with added PVP-K30 (3 mg/mL): (a) as prepared; (b) after heat treatment.

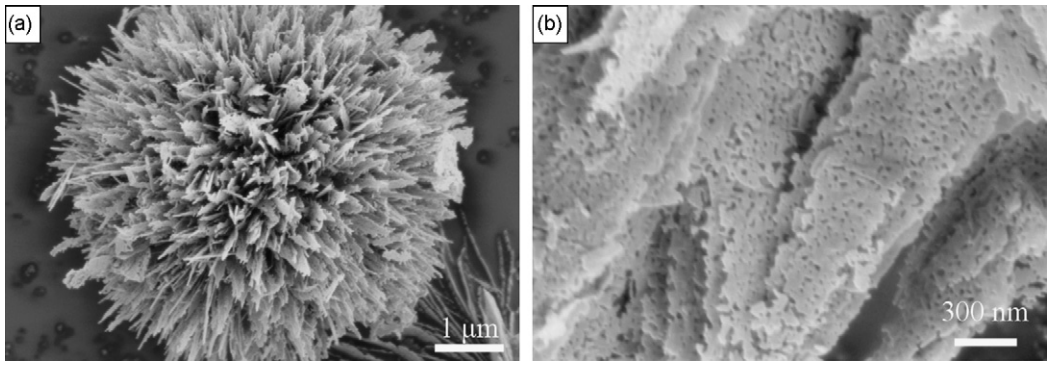

Fig. 6. FE-SEM micrograph of a sample prepared with addition of PVP-K30 (3 mg/mL) after 4 h of synthesis and with additional heat treatment up to 600 °C.

the XRD spectrum (Fig. 5a) it is evident that the product is not well crystallized. This confirms the results obtained from the IR observations. The major peaks (Fig. 5a) correspond to $Zn_5(OH)_6(CO_3)_2$ (JCPDS 19-1458, zinc hydroxide carbonate, hydrozincite). After heating at 600 °C sharp diffraction lines corresponding to well crystallized ZnO (JCPDS 36-1451) appear (Fig. 5b). Very similar XRD spectra before and after heat treatment were also obtained for samples prepared without any additives (not presented in the paper).

The average crystallite size for the sample with added PVP-K30 before and after heating were calculated by the Scherrer equation $\varepsilon = K\lambda/(B\cos\theta)$ and the lattice strain by the tangent equation Strain $= B/(4\tan\theta)$, where K (shape factor) is 0.9 and B is structural broadening, which is the difference in integral profile width between the standard and sample (in the Scherrer equation $B = B_{obs} - B_{std}$ and for lattice strain $B = (B_{obs}^2 - B_{std}^2)^{1/2}$).[21] According to the Scherrer analysis the average crystallite size in the sample before heating was 52 nm and the mean lattice strain was 0.29%. After heating the average crystallite size decreased to 27 nm, while the mean lattice strain slightly increased to 0.33%. The results obtained after heat treatment are in good agreement with calculated results obtained by Lima et al.[22] They reported an average crystallite size around 30 nm and a mean lattice microstrain around 0.276% for ZnO treated at 600 °C.

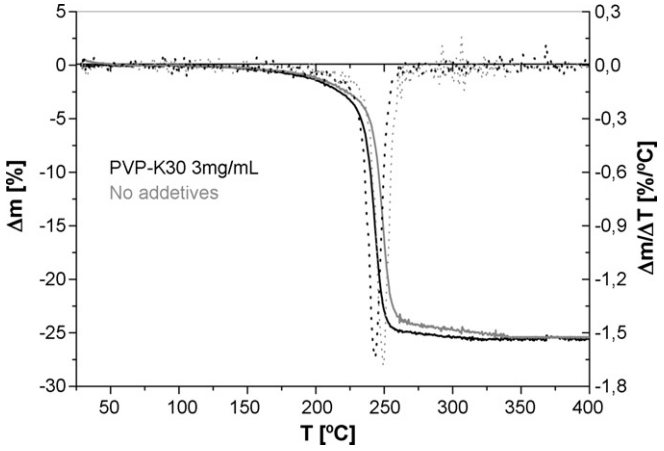

Fig. 7. Evolution of weight loss versus temperature in non-isothermal TG tests of two precipitated zinc hydroxide carbonate samples (continuous lines represent TG curves while dashed lines represent DTG curves).

Since the calculated size of the crystallites is much smaller than the particles observed by FE-SEM (Fig. 1b), we presumed that the precipitated particles are agglomerates of smaller crystallites. On the other hand, broadening of diffraction peaks may also result due to strains present in the particles. Increased lattice strain after annealing was attributed to the mass loss due to outflow of CO_2 and H_2O. Generally the size of the particles observed by FE-SEM remains practically the same on the microscale during heat treatment (Fig. 6a). However, a closer look of the particle surface after heat treatment revealed smaller crystallites forming a nanoporous structure (Fig. 6b). In consideration of the fact that annealing of the precipitated zinc hydroxide carbonate causes a substantial mass loss with minimal particle size change on the micrometer scale, the likelihood of increased lattice strain becomes more certain.

The nanoporosity of the particles upon heat treatment is reflected in their increased surface area. The specific surface area

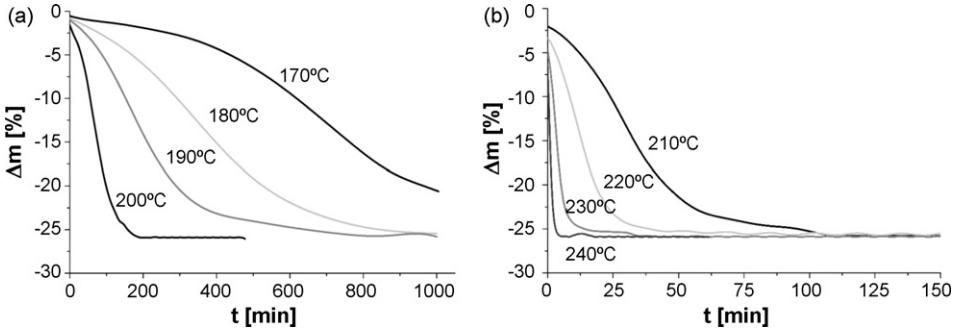

Fig. 8. Isothermal treatment of zinc hydroxide carbonate (sample with PVP-K30 addition) at various temperatures: (a) 170–200 °C; (b) 210–240 °C.

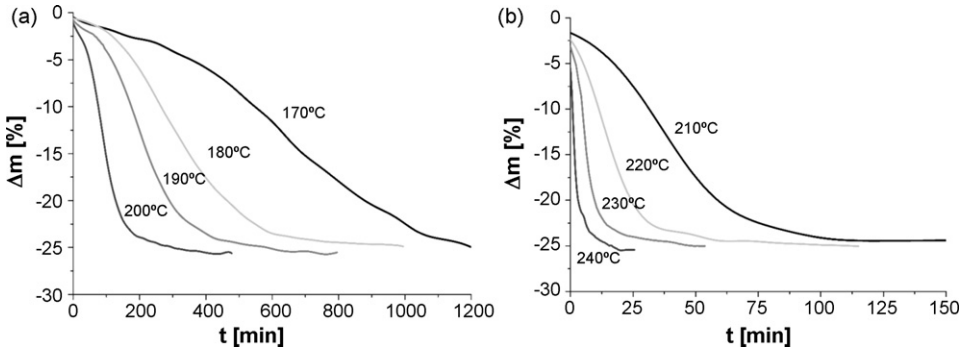

Fig. 9. Isothermal treatment of zinc hydroxide carbonate (sample without additives) at various temperatures: (a) 170–200 °C; (b) 210–240 °C.

of the sample with addition of PVP-K30 (3 mg/mL) increased from 16 m^2/g before to 40 m^2/g after heat treatment. This is an interesting result since in literature[23,24] it is reported that surface area values for ZnO particles decrease after heat treatment.

The thermal decomposition of the prepared zinc hydroxide carbonate ($Zn_5(OH)_6(CO_3)_2$) was examined by non-isothermal TG tests in a steady flow of Ar as carrier gas (Fig. 7). According to the results in Fig. 7 the prepared zinc hydroxycarbonates (with the addition of PVP-K30 or without additives) decomposed in only one relatively sharp step, with a peak decomposition rate at 244 and 250 °C, respectively. In both cases the weight loss increased only slightly in the temperature interval up to 200 °C. Above this temperature the decomposition rate became fast. However, when the two TG curves were compared, the same degree of thermal decomposition of the sample without additives lagged behind by approximately 10 °C. Up to ~290 °C almost 98% of the theoretical decomposition (25.2% overall mass loss) was reached in the case of the sample with PVP-K30 addition, while for the sample without additives at the same temperature only 95% decomposition occurred (the theoretical decomposition for the reaction $Zn_5(OH)_6(CO_3)_2 \rightarrow 5ZnO + 2CO_2 + 3H_2O$ was calculated to be 25.88%). H_2O and CO_2 as the only volatile products of the above mentioned thermal decomposition were further confirmed by the EGA analysis. Evolution of both gases followed the TG curve almost perfectly, suggesting that de-hydroxylation and decarboxylation proceeded simultaneously with no intermediate state of anhydrous $ZnCO_3$ formation.

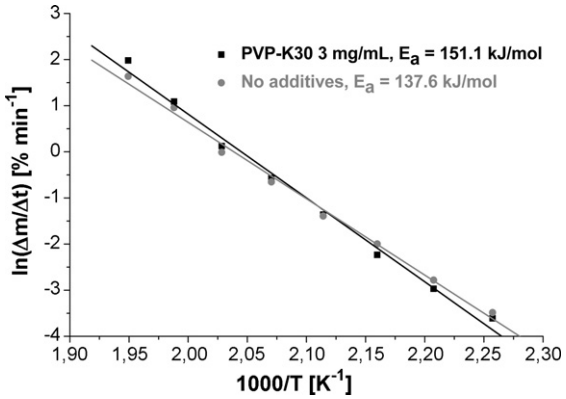

Fig. 10. Arrhenius plots for thermal decomposition of prepared zinc hydroxide carbonate.

Isothermal decomposition studies were performed for both samples in the temperature range 170–240 °C (Figs. 8a and b and 9a and b). Since the isothermal period always followed the non-isothermal sample treatment, the weight loss measured at time 0 in Figs. 8 and 9 corresponds to the decomposition of the sample reached at the end of the non-isothermal period. As expected, the higher predetermined temperature of isothermal treatment shortened the time required to achieve a certain degree of thermal decomposition.

Data obtained from the decomposition curves (as peak decomposition rates vs. reciprocal temperature) are presented in Fig. 10. From the slope of a straight line connecting the points in Fig. 10 the apparent decomposition activation energy for samples with PVP-K30 addition and without additives can be calculate as 151.1 and 137.6 kJ/mol, respectively. The calculated values of the apparent activation energy agree well with the data published by Kanari et al.[15] For thermal decomposition of two different zinc hydroxide carbonates they proposed values of the activation energy of 132 ± 5 and 153 ± 4 kJ/mol.

4. Conclusion

Porous ZnO particles in the shape of spherical chrysanthemums were synthesized in two steps. First zinc hydroxide carbonate was formed, and after subsequent heating up to 600 °C in an Ar atmosphere the products was transformed into ZnO without change in morphology. At the same time, the crystallite size of the samples decreased from 52 to 27 nm after heating, while the mean lattice strain changed from 0.29% to 0.33%. The surface area increased from 16 to 40 m^2/g as a consequence of the newly formed nanoporous surface.

The most homogeneous system was produced in the presence of PVP-K30 (3 mg/mL). At the beginning of the reaction the particles obtained were composed of nanowires. With time the nanowires grow in one dimension—becoming wider and more leaf-like.

The precipitated zinc hydroxide carbonate (with the addition of PVP-K30 or without additives) decomposed in only one relatively sharp step as revealed by TG tests. However, PVP-K30 addition triggers thermal decomposition at approximately 10 °C lower temperatures. From isothermal decomposition studies the apparent decomposition activation energy for samples with PVP

addition and without additives were calculated as 151.1 and 137.6 kJ/mol, respectively.

Acknowledgement

The authors gratefully acknowledge the financial support of the Ministry of Higher Education, Science and Technology of the Republic of Slovenia, and the Slovenian Research Agency (programme P1-0030).

References

1. Rensmo, H., Keis, K., Lindstrom, H., Sodergren, S., Solbrand, A., Hagfeldt, A. *et al.*, High light to energy conversion efficiencies for solar cells based on nanostructured ZnO electrodes. *J. Phys. Chem. B*, 1997, **101**, 2598–2601.
2. Preis, W., Konigsberger, E. and Gamsjager, H., Solid-solute phase equilibria in aqueous solution. XII. Solubility and thermal decomposition of smithsonite. *J. Sol. Chem.*, 2000, **29**, 605–618.
3. Tang, Z. K., Wong, G. K. L., Yu, P., Kawasaki, M., Ohtomo, A., Koinuma, H. *et al.*, Room-temperature ultraviolet laser emission from self-assembled ZnO microcrystallite thin films. *Appl. Phys. Lett.*, 1998, **72**, 3270–3272.
4. Huang, M. H., Mao, S., Feick, H., Yan, H., Wu, Y., Kind, H. *et al.*, Room-temperature ultraviolet nanowire nanolasers. *Science*, 2001, **292**, 1897–1899.
5. Pan, Z. W., Dai, Z. R. and Wang, Z. L., Nanobelts of semiconducting oxides. *Science*, 2001, **291**, 1947–1949.
6. Liu, B. and Zeng, H. C., Hydrothermal synthesis of ZnO nanorods in the diameter regime of 50 nm. *J. Am. Chem. Soc.*, 2003, **125**, 4430–4431.
7. Guo, L., Ji, Y. L. and Xu, H., Regularly shaped single-crystalline ZnO nonorods with wurtzite structure. *J. Am. Chem. Soc.*, 2002, **124**, 14864–14865.
8. Rodriguez-Paez, J. E., Caballero, A. C., Villegas, M., Moure, C., Duran, P. and Fernandez, J. F., Controlled precipitation methods: formation mechanism of ZnO nanoparticles. *J. Eur. Ceram. Soc.*, 2001, **21**, 925–930.
9. Reverchon, E., Della Porta, G., Sannino, D. and Ciambelli, P., Supercritical antisolvent precipitation of nanoparticles of a zinc oxide precursor. *Powder Tech.*, 1999, **102**, 127–134.
10. Castelano, M. and Matijević, E., Uniform colloidal zinc compounds of various morphologies. *Chem. Mater.*, 1989, **1**, 78–82.
11. Musić, S., Popović, S., Maljković, M. and Dragčević, Đ., Influence of synthesis procedure on the formation and properties of zinc oxide. *J. Alloys Compd.*, 2002, **347**, 324–332.
12. Liu, Y., Zhou, J., Larbot, A. and Persin, M., Preparation and characterization of nano-zinc oxide. *J. Mater. Process. Technol.*, 2007, **189**, 379–383.
13. Dollimore, D., France, J. A., Krupay, B. W. and Witehead, R., Kinetic aspects of the thermal decomposition of zinc carbonate. *Thermochim. Acta*, 1980, **36**, 343–349.
14. Chen, J., Zhao, R., Jiang, H., Li, Y. and Bao, G., Thermodecomposition of zinc carbonate hydroxide hydrate powders of different particle size and sample mass. *Transact. Nonferr. Metal. Soc. Chin. (Engl. Ed.)*, 1998, **8**, 149–153.
15. Kanari, N., Mishra, D., Gaballah, I. and Dupre, B., Thermal decomposition of zinc carbonate hydroxide. *Thermochim. Acta*, 2004, **410**, 93–100.
16. Li, Z., Shen, X., Feng, X., Wang, P. and Wu, Z., Non-isothermal kinetics studies on the thermal decomposition of zinc hydroxide carbonate. *Thermochim. Acta*, 2005, **438**, 102–106.
17. Crnjak Orel, Z., Maček, J., Marinšek, M. and Pejovnik, S., Coprecipitation of copper/zinc compounds in metal. *J. Eur. Ceram. Soc.*, 2007, **27**, 415–455.
18. Stoilova, D., Koleva, V. and Vassileva, V., Infrared study of some synthetic phases of malachite ($Cu_2(OH)_2CO_3$)–hydrozincite ($Zn_5(OH)_6(CO_3)_2$) series. *Spectrochim. Acta A*, 2002, **58**, 2051–2059.
19. Hayashi, S., Nakamori, N. and Kanamori, H., Generalized theory of average dielectric constant and its application to infrared absorption by ZnO small particles. *J. Phys. Soc. Jpn.*, 1979, **46**, 176–183.
20. Verges, A. M., Mifsud, A. and Serna, C. J., Formation of rod-like zinc oxide microcrystals in homogeneous solution. *J. Chem. Soc. Faraday Trans.*, 1990, **86**, 959–963.
21. PANalytical B.V., X'Pert HighScore, ver. 2.1b, Almelo, The Netherlands.
22. Lima, S. A. M., Sigoli, F. A., Jafelicci Jr., M. and Davolos, M. R., Luminescent properties and lattice defects correlation on zinc oxide. *Int. J. Inorg. Mater.*, 2001, **3**, 749–754.
23. Musić, S., Dragčević, Đ., Maljković, M. and Popović, S., Influence of chemical synthesis on the crystallization and properties of zinc oxide. *J. Mater. Chem. Phys.*, 2002, **77**, 521–530.
24. Audebrand, N., Auffrédic, J. P. and Louër, D., X-ray diffraction study of the early stages of the growth of nanoscale zinc oxide crystallites obtained from thermal decomposition of four precursors. general concepts on precursor-dependent microstructural properties. *Chem. Mater.*, 1998, **10**, 2450–2461.